Article for *J. Phys. Chem. B* (2018; transferred from *JPCL*)

Watching an Engineered Calcium Biosensor Glow: Altered Reaction Pathways before Emission

*Sean R. Tachibana, Longteng Tang, Liangdong Zhu, Weimin Liu,[§] Yanli Wang, and Chong Fang**

Department of Chemistry, Oregon State University, Corvallis, Oregon 97331, United States

Corresponding Author

*E-mail: Chong.Fang@oregonstate.edu. Phone: 541-737-6704.

ABSTRACT. Biosensors have become an indispensable toolset in life sciences. Among them, fluorescent protein based biosensors have great biocompatibility and tunable emission properties, but their development is largely trial and error. To facilitate rational design, we implement tunable femtosecond stimulated Raman spectroscopy (FSRS), aided by transient absorption and quantum calculations, to elucidate the working mechanisms of a single-site Pro377Arg mutant of an emission ratiometric Ca^{2+} biosensor based on a GFP-calmodulin complex. Comparisons with the parent protein and the Ca^{2+}-free/bound states unveil more structural inhomogeneity yet an overall faster excited state proton transfer (ESPT) reaction inside the Ca^{2+}-bound biosensor. The correlated photoreactant and photoproduct vibrational modes in the excited state reveal more chromophore twisting and trapping in the Ca^{2+}-bound state during ESPT, and the largely conserved chromophore dynamics in the Ca^{2+}-free state from parent protein. The uncovered structural dynamics insights throughout an ESPT reaction inside a calcium biosensor provide important design principles in maintaining a hydrophilic, less compact, and more homogeneous environment with directional H-bonding (from the chromophore to surrounding protein residues) via bioengineering methods to improve the ESPT efficiency and quantum yield while maintaining photostability.

I. INTRODUCTION

Biosensor technology creates powerful tools to probe and understand complex biological processes in real time, which has greatly advanced bioimaging and life sciences.[1-6] Among them, fluorescent protein (FP) biosensors utilize the photosensitive FP unit as part of a nanomachine to image cellular components of interest due to their high signal-to-noise ratios, biocompatibility, versatile engineerability, and tunable emission properties that span the UV to visible range. The large Stokes shift between absorption and emission of the FP-based biosensors stems from excited state proton transfer (ESPT) that allows the protein chromophore to relax to a lower energy state before radiative emission. Therefore, ESPT is a crucial step in governing their main functions,[7-11] which represents an archetypal biomolecular system to reveal the structure-function relationships on their intrinsic time scales. By understanding the ESPT reaction and competing pathways on the native femtosecond (fs) to picosecond (ps) time scales, one can rationally suggest specific single or multi-site mutations in tailoring new FPs and FP-based biosensors for advanced applications. The fundamental knowledge about how a chromophore interacts with its local environment inside a protein matrix also affords a rare opportunity to investigate conformational states and dynamics, energy relaxation pathways, and key atomic motions when a bioluminescent complex is in action.

In this study, we synergistically implemented the tunable femtosecond stimulated Raman spectroscopy (FSRS),[12-14] transient absorption (TA), and quantum calculations[15] to uncover the effects of a single-site Pro377Arg (P377R) mutation of a parent green fluorescent protein (GFP) based calcium biosensor GEM-GECO1 (GECO stands for genetically encoded calcium indicator for optical imaging).[16,17] The integral platform of electronic and vibrational spectroscopies, aided by normal mode assignment using computational chemistry methods, enables us to reveal the structure-energy-function relationships of a biomolecular system on the basis of time-resolved

spectra starting from the time zero of electronic excitation. For the recently engineered GECO series, this platform has been proven effective in dissecting the fluorescence mechanisms.[17-20]

Since calcium ions play essential regulatory roles in cellular systems from gene expression, metabolism, hormone release, neuron firing, muscle contraction, to pathology, the importance to develop better calcium biosensors cannot be overstated. These fluorescent biosensors consist of a circularly permuted GFP (cpGFP), an adjacent calmodulin (CaM) subunit and a chicken kinase M13 peptide as its binding client.[2,16] The cpGFP, unlike wtGFP, has an opening in the β-barrel that exposes the phenolic end of the embedded serine-tyrosine-glycine (SYG) chromophore to the environment. During directed evolution,[16] one residue stands out to be crucial for blue emission from the Ca^{2+}-bound biosensor: Pro377 in the CaM subunit that largely shields the β-barrel opening and inhibits ESPT from the cpGFP chromophore. On the basis of a previous report that the Pro377Arg (P377R) mutation converts the parent biosensor from green-blue emission ratiometric to green excitation ratiometric,[19] the elucidation of fluorescence modulation mechanisms of this engineered calcium ion (Ca^{2+}) biosensor requires a much improved sensitivity to track the photoproduct species I* after excitation of the photoreactant species A* in different local environments, induced by the Ca^{2+}-binding events at allosteric sites away from the photosensitive chromophore (see Figure 1 for illustration).

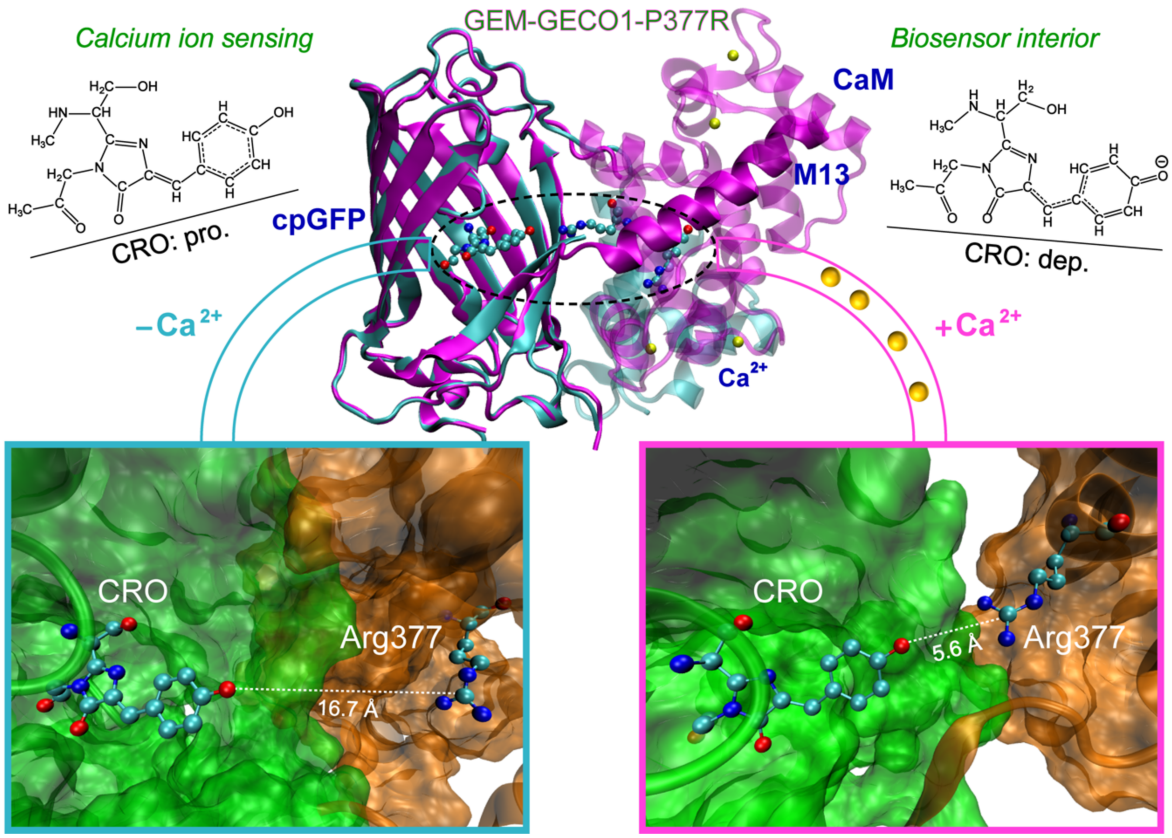

Figure 1. Protein structural illustration of the Ca^{2+}-free (cyan) and bound (magenta) GEM-GECO1-P377R calcium biosensor. The four Ca^{2+} ions bound to each biosensor are represented by yellow spheres. The SYG chromophore (CRO) and interfacial R377 residue (black dashed ellipse) are highlighted in the enlarged windows (lower panels), depicting the relative positions, orientations, and distances between the CRO phenolic oxygen in cpGFP (green) and R377 guanidinium carbon in the CaM (orange) subunit that notably change upon Ca^{2+} binding. The chemical structures of the protonated (pro.) and deprotonated (dep.) chromophores are also shown.

Given the photoresponse of the biosensor spanning multiple time scales, femtosecond transient absorption (fs-TA) is an effective first step to bring the steady-state electronic spectroscopy (e.g., UV/Visible absorption and fluorescence) into the time domain and starting from the time zero of photoexcitation. The excited-state electronic dynamics such as excited state absorption (ESA,

$S_1 \rightarrow S_n$), stimulated emission (SE, $S_1 \rightarrow S_0$), and ground state bleaching (GSB) provide a holistic picture of the potential energy surface (PES) involving the excited or relaxed chromophore in its microenvironment.[21] In practice, FSRS can be readily achieved in the same setup as fs-TA by incorporating an additional picosecond (ps) Raman pump to stimulate a Raman scattering process in a resonantly or pre-resonantly enhanced excited state population (sometimes even at off-resonant conditions but with a reduced signal-to-noise ratio), tracking the vibrational dynamics of interest.[10,22,23] Conventional FSRS spectrally filters the 800 nm laser output as Raman pump to overlap with a broad ESA band of FPs, enhancing the photoreactant in S_1.[10,17] Tunable FSRS expands research capability by positioning the Raman pump across a wide range so transient excited state species can be selectively enhanced on molecular time scales.[18,19,24,25] In comparison to the time-resolved IR studies on proteins,[26-28] the main experimental observables for FPs and FP-based biosensors in tunable FSRS are the vibrational dynamics of the chromophore immediately following electronic excitation, which underlie the protein main function in emitting light.

II. MATERIALS AND METHODS

A. Protein sample preparation. The GEM-GECO1-P377R biosensor (referred as P377R) sample was synthesized according to previously reported procedures, which started with *E. coli* DH10B cells (Invitrogen) transformed using the pTorPE plasmid with 6-histadine-tagged GEM-GECO1 protein.[16,17] For the P377R mutation, synthetic DNA oligonucleotides (Integrated DNA Technologies) and QuikChange Lighting Single kit (Agilent Technologies) were used. The final P377R protein samples were prepared in pH=7.2 MOPS buffer solution with 10 mM EGTA (Ca^{2+}-free) and 10 mM Ca-EGTA (Ca^{2+}-bound). The steady-state electronic absorption and emission spectroscopy is performed at room temperature using a Thermo Scientific Evolution 201 UV-Visible (UV-Vis) and a Hitachi F-2500 fluorescence spectrophotometer, respectively.

B. Femtosecond transient absorption (fs-TA). Our ultrafast laser source originates from a regenerative amplifier (Legend Elite-USP-1K-HE) seeded by a mode-locked Ti:Sapphire oscillator (Mantis-5, Coherent, Inc.). The fundamental pulse (FP) at 800 nm has ~35 fs duration, ~4 mJ energy, and 1 kHz repetition rate. About 75 mW of the FP goes through a β-barium borate (BBO) crystal for second harmonic generation to obtain the 400 nm pulse, followed by temporal compression using a prism pair (Suprasil-1, CVI Melles Griot). Its intensity is attenuated to ~0.2 mW to act as the actinic pump. About 25 mW of the FP passes through a pinhole and a neutral density filter before being focused on a 2-mm-thick *Z*-cut sapphire plate to generate a supercontinuum white light (SCWL) as the probe (ca. 430—700 nm).[18,23] The P377R sample concentration was made to reach OD=1/mm at 400 nm (also for femtosecond Raman measurement, see below). The protein biosensor solution was housed in a 1-mm-pathlength quartz flow cell (48-Q-1, Starna Cells) using a peristaltic pump, to minimize photodamage of the sample as well as reduce thermal effect during data collection. The pump and probe pulses focus at the sample while the time delay (up to 600 ps in this work) between them is regulated by a motorized delay stage (NRT150, Thorlabs, Inc.) where the pump beam traverses. We also performed a TA measurement with a compressed probe using a chirped mirror pair (DCM-9, 450—950 nm, Laser Quantum, Inc.). With the reduced pulse duration to ~50 fs, the main dynamics of interest remain unchanged, yet the bluer ESA region (see Figure 2b below) gets cut off due to the DCM-9 optical coating. Therefore, the fs-TA data in Figures 2b and 3 in main text were collected without the chirped mirror pair to analyze the broader spectral region and compare the excited state proton transfer (ESPT) dynamics on the ps or longer time scales.

C. Tunable femtosecond stimulated Raman spectroscopy (FSRS). The recently developed tunable FSRS setup in our laboratory has been reported.[12-14,23] In brief, half of the aforementioned

laser FP is used to power the fs actinic pump, the picosecond (ps) Raman pump, and the fs Raman probe. The tunable (~480—750 nm) Raman pump is achieved by a two-stage ps noncollinear optical parametric amplifier (NOPA), pumped by a ps 400 nm pulse out of a homebuilt second harmonic bandwidth compressor (SHBC).[12] Based on the electronic profiles of P377R biosensor, we tuned the Raman pump to 553 nm (~4 μJ, ~2 ps duration) to achieve pre-resonance condition with both the photoreactant and photoproduct TA bands while keeping the 400 nm actinic pump (0.1—0.2 μJ pulse energy),[23,25] to compare with conventional FSRS wherein the 800 nm Raman pump was used.[13,19] A control experiment using a 580 nm Raman pump led to a much reduced signal-to-noise ratio for the deprotonated chromophore species of interest, hence confirming the advantage of using the 553 nm Raman pump for pre-resonance Raman enhancement.[19,23] The fs broadband probe (ca. 560—630 nm) is generated by focusing ~2 μJ of the FP onto a 2-mm-thick sapphire plate (see above) and selecting the target region from the SCWL. All three incident pulses are focused to overlap at the sample spot in a 1-mm-pathlength flow cell (see above) that ensured sample integrity during a typical FSRS experiment lasting for ~2.5 hours. The FSRS signal collinear with the Raman probe is dispersed by a 1200 grooves per mm grating at 500 nm blaze in a spectrograph (Acton SpectraPro SP-2356, Princeton Instruments) before being imaged on a CCD array camera (PIXIS:100F, Princeton Instruments). Fifteen excited-state data sets were collected and within each data set, 1500 stimulated Raman spectra were averaged at each time delay point (>75 time points across the detection time window of 600 ps) by the LabVIEW custom-made suite of programs. The UV/Vis spectra were checked before and after the excited state TA and FSRS experiments with 400 nm pump to confirm the sample integrity (i.e., within 5%/10% spectral difference for the Ca^{2+}-free/bound P377R absorption profile, see Figure 2a for example).

III. RESULTS AND DISCUSSION

To achieve a high contrast for Ca^{2+} imaging, a ratio of excitation ratios can be taken due to the small deprotonated (B form) absorbance in the Ca^{2+}-bound state (Figure 2a). Using conventional FSRS, the hydrophilic Arg377 was found to create a less homogeneous chromophore environment inside the Ca^{2+}-bound biosensor with A* decay time constants of ~16 and 90 ps, which differ from the single time constant of 36 ps in the Ca^{2+}-free biosensor.[19] However, an important question regarding the biosensor mechanism remains: which characteristic nuclear motions respond to the key single-site mutation that alters the photochemical reaction pathways and outcomes? Such mechanistic insights require a structural dynamics technique that can track transient molecular species during (not just before and after) a photoinduced process.[14] The main experimental evidence to support any rational design principles need to include the site-specific information on molecular time scales, which typically span the fs to ps range when primary structural events occur and govern the molecular fate as well as the "downstream" macroscopic functions of interest.[13,17,29]

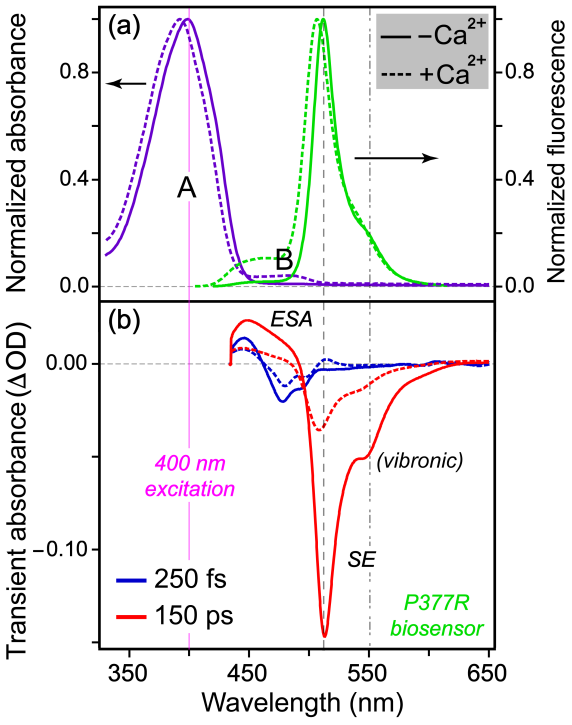

Figure 2. Electronic spectroscopy of the P377R biosensor in aqueous buffer solution. (a) Normalized steady-state absorption (violet) and emission (green) spectra of the Ca^{2+} free (solid) and bound (dashed) states. The protonated and deprotonated chromophore is denoted by A and B, respectively. (b) Fs-TA spectra at 250 fs (blue) and 150 ps (red). The actinic pump was set to 400 nm (vertical magenta line). The main SE band and a prominent red shoulder are marked by the vertical dashed and dash-dotted lines, likely indicative of vibronic coupling. The evolution from the A* SE peak at ~478 nm (blue dip) to the I* SE peak at ~510 nm (red dip) is apparent.

A. Steady-State Absorption and Fluorescence Spectroscopy. Figure 2a displays the steady-state absorption and emission spectra that are reminiscent of a GFP chromophore except that the B form has a much smaller contribution in the biosensor than wtGFP.[7,8,10] A 400 nm actinic pump was selected for TA and FSRS to effectively pump the dominant A form. Interestingly, the Ca^{2+}-bound biosensor shows an increased B absorption peak at ~480 nm and also an increased A* emission peak at ~460 nm which indicates structural inhomogeneity in the ground and excited state,[17,30] while its absorption and emission peaks (392 and 506 nm) are both blue shifted from the Ca^{2+}-free counterparts (399 and 512 nm). Such a blue shift of electronic features upon Ca^{2+} binding is commonly observed in the GECO family, likely due to an increase of electrostatic interaction stabilizing the photoacidic chromophore better in the ground state (S_0) than that in the excited state (e.g., S_1) with a reduced dipole after the photoinduced ultrafast intramolecular charge transfer across the chromophore two-ring conjugated system.[16,17,19,31-33]

B. Time-Resolved Electronic Spectroscopy. Upon 400 nm excitation, Figures 2b and 3 provide clear evidence that some chromophore S_0 populations reach a transient S_1 state, and the initial protonated photoreactant (A*) converts to a deprotonated photoproduct (I*) on ultrafast time

scales. Robust assignment of two chromophore species (i.e., change of protonation states) before and after ESPT is corroborated by a close match between the A* and I* SE peaks and fluorescence peaks (Figure 2). At early times (e.g., 250 fs), the main negative peak at 478/479 nm for the Ca^{2+}-free/bound biosensor corresponds to the A* SE band, located to the red side of the A* fluorescence peak (~460 nm), which is in accord with the aforementioned charge transfer characteristics in the transient electronic excited state.[11,32,34] Since the ground state B population is very small with an absorption peak at ~480 nm, we do not expect a significant GSB contribution from the B species after 400 nm excitation. At late times (e.g., 150 ps), the Ca^{2+}-free/bound biosensor SE band grows and red shifts to 513/508 nm that is attributed to I* after ESPT, confirmed by the spontaneous emission peaks at 512/506 nm.

In addition, a prominent red shoulder appears in both fluorescence and SE bands. To elucidate its origin, we took a 1-nm slice from the main SE band (513/508 nm) and shoulder (550/544 nm) for the Ca^{2+}-free/bound biosensors (see Figure S1 in the Supporting Information), which exhibit nearly identical dynamics between their respective main SE band and red shoulder, indicating that both peaks arise from the same transient deprotonated chromophore species. In particular, the shoulder observed in the fluorescence band is associated with a vibrational mode in S_0 that is coupled to the downward electronic transition, whereas the SE shoulder could involve a similar vibrational mode in S_1 as the I* species relax in a non-equilibrium electronic excited state.[25,35,36] The choice of tunable Raman pump at the red side of main SE band potentially enhances the vibrational modes associated with these vibronic transitions (see below).

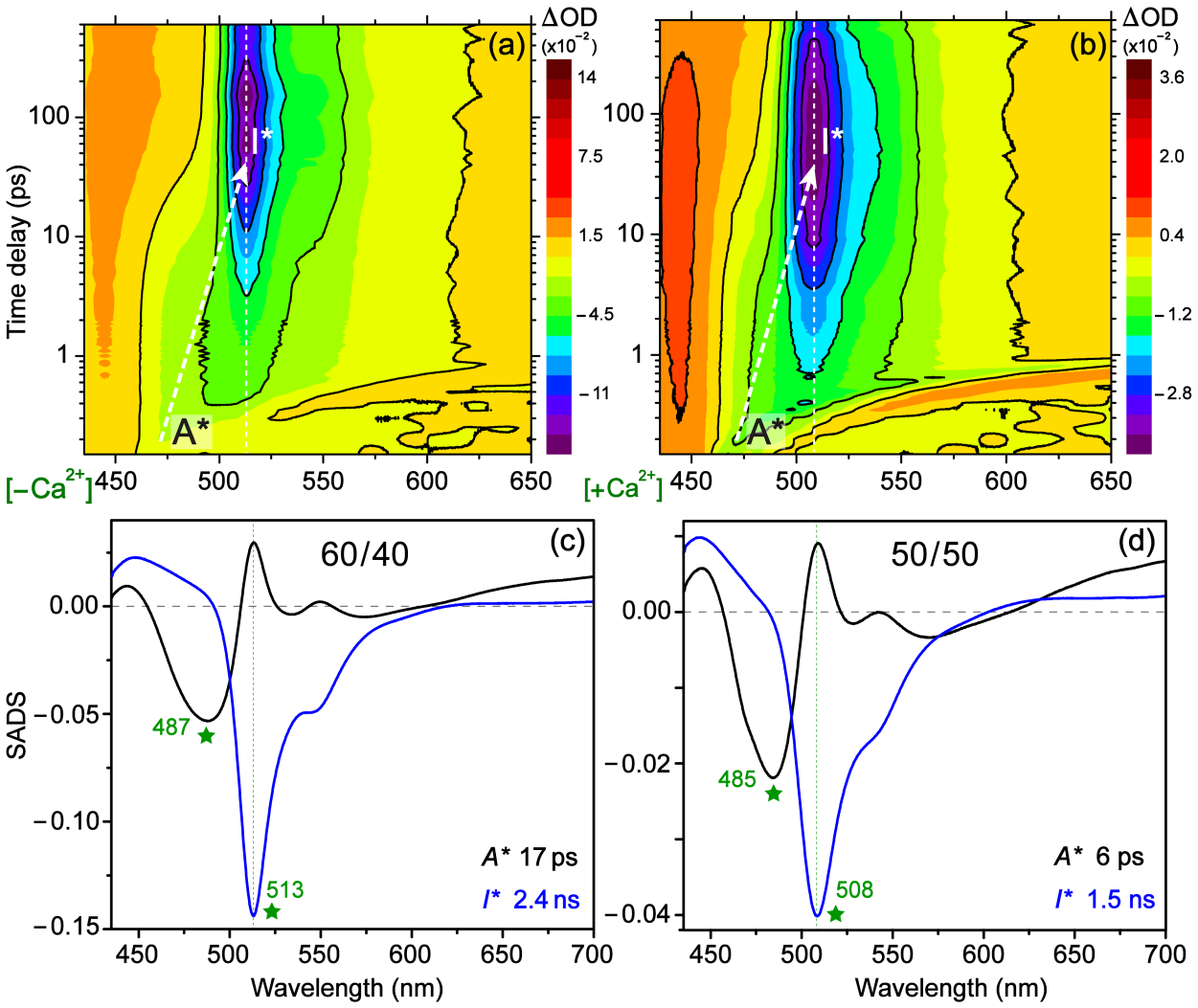

Figure 3. Fs-TA contour plot of the Ca^{2+}-free (a) and bound (b) states after 400 nm excitation. The A*→I* transition through ESPT reaction is highlighted by the white dashed line across SE bands. Target analysis of the Ca^{2+}-free (c) and bound (d) states adopts a two-component (A*→I*) model. To correct for fluorescence background (FB), the optimal A*/FB initial population is denoted in black. The 17 ps ESPT time constant and 2.4 ns green fluorescence lifetime were derived for the Ca^{2+}-free state whereas the Ca^{2+}-bound state analysis converges to lifetimes of 6 ps and 1.5 ns.

The experimental TA spectra are typically convoluted due to overlapping electronic bands associated with multiple populations (Figure 3a and b). To better understand how each population

evolves with time, global and target analyses are typically used to dissect complex systems.[37] For the Ca^{2+}-free and bound biosensors, multiple components were tested via target analysis (see Figure S2) to examine the validity of signal deconvolution. Figure 3c and d present the simplest reasonable model (i.e., two-component sequential model, A*→I*→I) with the 17/6 ps and 2.4/1.5 ns time constants for the Ca^{2+}-free/bound states, respectively. The initial process corresponds to the main ESPT reaction with a clear transition of SE bands (i.e., A*→I*), revealing that the hydrophilic Arg377 in the Ca^{2+}-bound biosensor facilitates a faster ESPT channel. The nanosecond process is associated with the green fluorescence lifetime as the SE band diminishes (i.e., I*→I). We note that a fluorescence background (FB) signal is present at negative time points due to an intrinsic difference of the probe spectrum between the pump on and pump off cases with laser repetition rate at 1 kHz, while the CCD camera records the signal non-stop within the 1 ms data collection window for each laser shot. To correct for FB contribution and elucidate the dynamic ESPT reaction pathway, an initial population ratio (A*/FB) of 60/40 and 50/50 was optimized to least-squares fit the TA data of the Ca^{2+}-free/bound states to retrieve the target analysis species.

C. Time-Resolved Vibrational Spectroscopy using Tunable FSRS. Because the main ESPT reaction occurs on the picosecond time scale, we implement the tunable FSRS methodology to track nuclear motions during the photoproduct formation. Using a Raman pump at 553 nm that is preresonant with the I* SE band at ~510 nm (Figure 3), we effectively capture the essence of ESPT because (1) it is the only pathway converting A* to I*, (2) the Raman pump is >40 nm away from the SE peak so the Raman-pump-induced depletion of I* population is insignificant,[23,38] (3) the observed vibrational dynamics of I* provide unambiguous information about the rise and decay of deprotonated chromophore species before returning to S_0. In Figure 4a and b, excited state FSRS contour plot of the Ca^{2+}-free/bound biosensor is contrasted with the buffer-subtracted ground state

spectra: the frequency and intensity change of the Raman modes between S_0 and S_1 is conspicuous. In particular, the ground state chromophore only exhibits one prominent peak at ~1565 cm^{-1}, while an array of peaks from ~700 to 1700 cm^{-1} manifest interesting dynamics (e.g., peak integrated intensity and center frequency, vide infra) in the excited state in close association with ESPT reaction (Figure 4) that warrants detailed analysis.

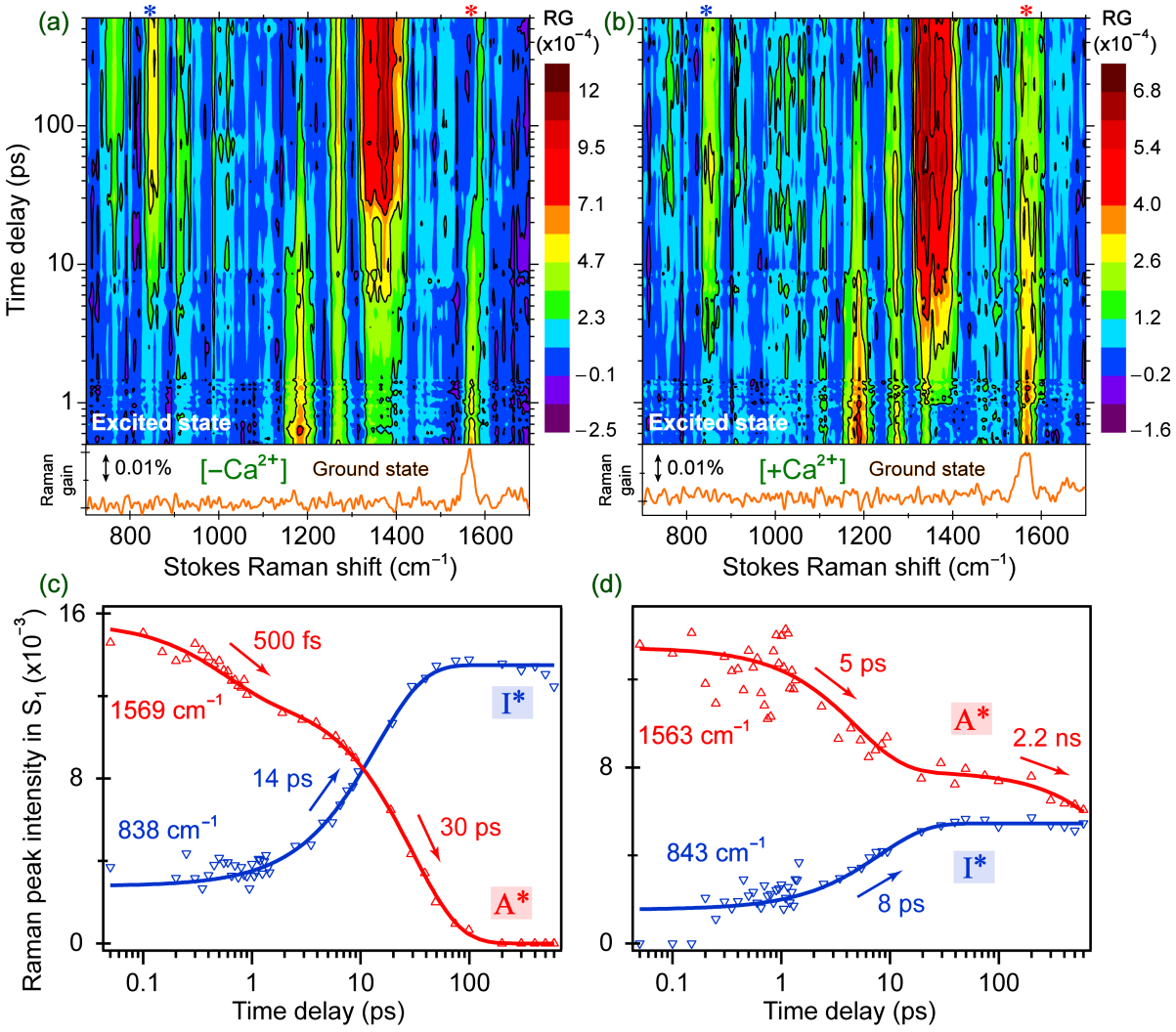

Figure 4. Tunable FSRS 2D contour plot of the Ca^{2+}-free (a) and bound (b) P377R biosensor from 10 fs to 600 ps with 400 nm actinic pump and 553 nm Raman pump. The ground state spectra are displayed below (orange). For vibrational intensity dynamics of the Ca^{2+}-free (c) and bound (d)

biosensor in S_1, the I* 838/843 cm^{-1} mode intensity rise (blue) is contrasted with the A* 1569/1563 cm^{-1} mode intensity decay (red) with the multiexponential fits in solid curves and time constants.

First, the Ca^{2+}-free and bound biosensors show similar peak positions and dynamic patterns (see Figure S3 for the raw experimental spectra with baselines drawn across the detection window). This is expected because they share the same SYG chromophore (see Figure 1 inset for the chemical structures with different protonation states) and both emit green light upon 400 nm excitation, and the major difference in the chromophore local environment is the proximity to an interfacial R377 residue located on a different protein subunit.[10,17,19] This allows an effective spectroscopic platform to track the chromophore response at the biosensor active site as the Ca^{2+}-binding events occur allosterically at the nearby CaM domain (Figure 1), and reveal key differences between the excited state vibrational motions.

Second, the I* modes at ~840, 860 and 1340 cm^{-1} appear earlier in Figure 4b than 4a, indicative of a faster ESPT channel in the Ca^{2+}-bound biosensor wherein the I* population rises with an 8 ps time constant (Figure 4d) versus 14 ps in the Ca^{2+}-free biosensor (Figure 4c, while the fit of the adjacent 860 cm^{-1} mode yields a similar 12 ps rise time constant). Quantum calculations show that the ~840 and 860 cm^{-1} modes mainly consist of the phenolic ring out-of-plane deformation (see Table S1) and the imidazolinone ring deformation,[24] respectively, hence these ring motions are a sensitive vibrational probe for the accumulation of I* species due to the increased electric polarizability over the two-ring system and pre-resonance enhancement (i.e., the I* SE peaks at ~510 nm while the Raman pump is at 553 nm, see Figure 2b). This dynamic trend also matches a previous report on the TYG chromophore in the Ca^{2+}-free/bound G-GECO1.1 biosensors, wherein tunable FSRS with a 529 nm Raman pump allowed the tracking of I* ~1370 cm^{-1} mode intensity rise with 42/22 ps time constants.[18] Notably, the Ca^{2+}-free over bound ratio of I* intensity rise time

constants (14 ps/8 ps ≈ 1.8) in the P377R biosensor matches that in the G-GECO1.1 biosensor (42 ps/22 ps ≈ 1.9). It is thus plausible that the protonated SYG chromophore is more prone to ESPT upon 400 nm photoexcitation than the TYG chromophore,[3,8] but the effect of Ca^{2+} binding on the ESPT rate is comparable in both biosensors.

Third, a faster reaction may lead to less complete ESPT if an inhomogeneous population consists of significant subpopulations that cannot undergo ESPT (e.g., trapped in A*). This point is evinced by the prolonged A* 1563 cm^{-1} mode intensity decay that differs from the I* 843 cm^{-1} mode intensity rise in the Ca^{2+}-bound biosensor (Figure 4d). The ~5 ps (with 43% amplitude weight in the least-squares fit) initial A* decay is an average of Franck-Condon (FC) relaxation and ESPT dynamics which is in accord with the ~8 ps I* rise. The much longer 2.2 ns (with 57% amplitude weight) A* decay likely reflects a mixture of fluorescence lifetime and nonradiative decay pathways so the trapped chromophore subpopulation could return to the ground state. Due to our experimental pre-resonance condition favoring the I* modes, the A* mode dynamics become more convoluted thus exhibiting averaged dynamics; the cleaner A* decay dynamics can be observed using conventional FSRS with an 800 nm Raman pump.[10,19] Using ultrafast vibrational spectroscopy, similar conformational inhomogeneity has been observed in a membrane protein environment due to a slower exchange between different H-bonding configurations.[26]

Fourth, the Ca^{2+}-free biosensor exhibits similar dynamics as the previous conventional FSRS results (Figure 4c).[19] Unlike the Ca^{2+}-bound state, the Ca^{2+}-free biosensor reveals a more homogeneous and efficient ESPT channel that allows the A* 1569 cm^{-1} mode decay to zero, suggesting that the resonance conditions for A* species diminish more dramatically as the Ca^{2+}-free biosensor chromophore undergoes ESPT reaction. It also shows that energy dissipation via competing pathways (e.g., nonradiative relaxation) is more significant in the Ca^{2+}-free case.

With this enhanced sensitivity for certain A* species, the initial 500 fs decay (with 41% amplitude weight) in Figure 4c shows the A* population moving out of the FC region[10,17,20] while the 30 ps decay (with 59% amplitude weight) represents an ensemble average of ESPT (~14 ps for the I* 839 cm^{-1} mode rise in Figure 4c) and other A* nonradiative relaxation processes on the tens of ps time scale.[20,39] We note that this 30 ps time constant is also retrieved from other A* modes at ~1155, 1183, and 1208 cm^{-1}. Since the fluorescent quantum yield for such biosensors is typically around 0.2 with 400 nm excitation,[16,17,20] the nonradiative relaxation channels effectively compete with ESPT on ultrafast time scales to deplete the A* population. This also explains the negligible A* spontaneous emission peak in the Ca^{2+}-free state (Figure 2a).

D. Characteristic Vibrational Motions Differ in the Ca^{2+} Free and Bound Biosensors. To better understand the observed and potentially functional structural motions of the biosensor chromophore, we analyze the Raman mode frequency dynamics in S_1 (Figure 5) to correlate with mode assignments aided by density functional theory (DFT) calculations. The peak doublet between 800 and 900 cm^{-1} displays different frequency dynamics upon Ca^{2+} binding. In the Ca^{2+}-free state, the ~838 cm^{-1} mode shows a 4 ps blue shift from 832 to 845 cm^{-1} (Figure 5a), which can be attributed to vibrational cooling (VC) within the I* state after the ultrafast ESPT reaction barrier crossing.[29,40-42] The adjacent 864 cm^{-1} mode exhibits a similar blue shift from 859 to 870 cm^{-1} with a 6 ps time constant. This observation represents the first time that a frequency shift is tracked in a photoproduct, instead of a photoreactant species or a mixed A*/I* species inside a protein pocket.[20,24,39] However, the Ca^{2+}-bound state does not show a clear blue shift (Figure 5b), which could be due to a less steep PES or competing pathways. In both the parent GEM-GECO1 (SYG chromophore, adjacent P377) and a related G-GECO1.1 biosensor (TYG chromophore, adjacent R377), the Ca^{2+}-bound state hosts a more twisted chromophore in the ground state.[24,43] To estimate

how twisting affects vibrational frequency in the excited state with reasonable computational costs, the DFT calculation of a 20º-twisted SYG chromophore was compared to the coplanar two-ring-system case (see Table S1 and Figure S4 for the pertinent mode assignment). For the calculated 828 cm^{-1} mode, the deprotonated chromophore shows a 4 cm^{-1} red shift as it twists by 20º. The close-in of the long side chain and positively charged R377 toward the chromophore in the Ca^{2+}-bound biosensor is expected to create a compact microenvironment (Figure 1) which allows the deprotonated chromophore after ESPT to further twist.[43] As a result, the VC-induced blue shift mixed with the twisting-induced red shift of the I* mode can lead to an overall stagnant Raman band center frequency (Figure 5b).

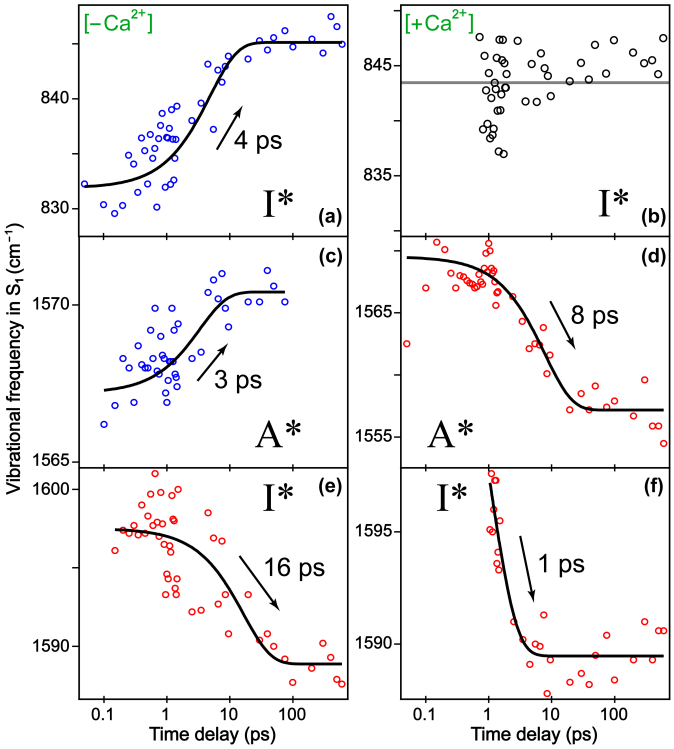

Figure 5. Excited state vibrational mode frequency dynamics of the P377R biosensor chromophore. In the Ca^{2+}-free state, the ~838 cm^{-1} I* mode, 1569 cm^{-1} A* mode, and 1594 cm^{-1} I* mode shifts are shown in (a), (c), and (e), respectively, with the single-exponential fits in solid black curves. Time constants are denoted. For comparison in the Ca^{2+}-bound state, the ~843 cm^{-1}

I* mode, 1563 cm^{-1} A* mode, and 1593 cm^{-1} I* mode shifts are shown in (b), (d), and (f), respectively. The ~1540 cm^{-1} I* shoulder peak affects the ~1569/1563 cm^{-1} A* peak dynamics.

When comparing the A* marker band frequency shift in the C=C, C=N, and C=O stretching region, the 1569/1563 cm^{-1} mode for the Ca^{2+}-free/bound biosensor is overlapped with the emerging I* modes at 1594/1593 and 1540/1540 cm^{-1}, essentially forming a "Y" spectral pattern as delay time increases (see Figure 4a and b). Given the challenge to retrieve mode dynamics from this congested high-frequency region,[24] we fit the spectra using multi-gaussian peaks and record the peak center frequencies. The 1540 cm^{-1} mode is dispersive in the FSRS spectra along with the 1300 cm^{-1} mode (Figure S3), indicating that both modes are coupled to the I* SE transition (i.e., vibronic coupling) thus involve hot luminescence pathways in the FSRS signal generation.[44,45] Furthermore, these specific modes project strongly along the ESPT reaction coordinate and are sensitive trackers for the I* formation.[10,18,39] Detailed fitting with dispersive line shape can also be performed[46] to retrieve more information about these modes, but the focus here is to monitor an adjacent mode frequency change. The frequency red shift from the ~1565 cm^{-1} A* mode has been observed in wild-type GFP and GEM-GECO1 biosensor (with a common SYG chromophore) after ESPT reaction and the resultant change of the H-bonding network around the nascent deprotonated chromophore (I*).[10,17] Such a red shift is observed for the Ca^{2+}-bound biosensor A* mode, ca. 1570$\rightarrow$1557 cm^{-1}, with a time constant of 8 ps (Figure 5d), matching the I* 843 cm^{-1} mode intensity rise time constant of 8 ps (Figure 4d), hence confirming their concomitant tracking of ESPT. This result shows that the shoulder peak with a dispersive line shape may not affect the apparent dynamics of a nearby dominant mode with a non-dispersive line shape, and the intensity "pulling" effect to exhibit a marker band red shift is still evident when the ESPT reaction occurs.

The general red shift trend of this vibrational mode frequency is also reproduced by TD-DFT calculations wherein the protonated chromophore motion at 1587 cm^{-1} becomes 1536 and 1572 cm^{-1} in the deprotonated chromophore (see Table S1).

In sharp contrast, the Ca^{2+}-free biosensor A* mode manifests a small blue shift, ca. 1567→1571 cm^{-1}, with a time constant of 3 ps (Figure 5c) that does not match the I* 839 cm^{-1} mode intensity rise time constant of 14 ps (Figure 4d). To rationalize this intriguing observation, we note that the ~1565 cm^{-1} marker band lasts much longer in the Ca^{2+}-bound than Ca^{2+}-free biosensor, so beyond tens of ps in the latter case, the I* modes at ~1540 and 1594 cm^{-1} dominate (Figure 4b). Indeed, the 1594 cm^{-1} I* mode (Figure 5e) exhibits a frequency red shift, ca. 1600→1588 cm^{-1}, with a time constant of 16 ps that is consistent with the ESPT rate in the Ca^{2+}-free biosensor. Our DFT calculations show that the deprotonated chromophore twisting leads to a mode frequency red shift of 3 cm^{-1} (i.e., 1581→1578 cm^{-1}, see Table S1) so the effect is additive to ESPT, i.e., the aforementioned intensity pulling from a nascent ~1540 cm^{-1} mode at the lower frequency side which also red shifts with the chromophore ring twisting (i.e., 1552→1546 cm^{-1}, see Table S1). In consequence, a blue shift for the "middle" 1569 cm^{-1} mode in the excited state (Figure 5c) could arise from a VC process in A* partially mixed with ESPT as well as the chromophore twisting-induced red shift of adjacent I* modes.

Furthermore, the 1593 cm^{-1} mode is attributed to I* due to its intensity rise after a short dwell of ~1 ps, while its frequency exhibits a 9 cm^{-1} red shift (ca. 1598→1589 cm^{-1}) with a ~1 ps time constant (Figure 5f) in the Ca^{2+}-bound state. This ultrafast time constant with a delayed onset of ~1 ps is unique among all the mode frequency dynamics in Figure 5, and is likely associated with the I* species responding to the rapidly rearranging bridge water molecules (i.e., between the chromophore phenolate oxygen end and the R377 side chain guanidinium end) on the typical

molecular water reorientation time scale.[38,47] This process is consistent with the deprotonated chromophore twisting in a more compact environment with certain H-bonding configurations in support of faster ESPT on the few ps time scale, so such a structural step adjusting the bridge water orientation is important to stabilize the nascent I* species and enlarge the "quantum box" for pertinent vibrational motions (i.e., leading to the observed mode frequency red shift). Meanwhile, a significant A* population does not undergo ESPT and remains trapped in the Ca^{2+}-bound biosensor, which explains the A* 1563 cm^{-1} mode intensity decay component of 2.2 ns in Figure 4d, as well as the increased A* spontaneous emission peak at ~460 nm (Figure 2a). In addition, our experiments showed that the Ca^{2+}-bound biosensor is more sensitive to laser irradiation (i.e., susceptible to photodamage reflected by a larger change of UV/Vis spectra before and after the FSRS data collection, see the Materials and Methods above) than the Ca^{2+}-free biosensor. This observation indicates that some trapped A* populations do not experience an efficient and/or effective relaxation pathway to achieve desirable molecular photoprotection properties for the Ca^{2+}-bound biosensor.[42,48]

E. Formulating the Design Principles of Fluorescent Biosensors from a Molecular Perspective. These mechanistic insights uncover a key design principle for the Ca^{2+} biosensor based on the cpGFP-CaM complex: reduce conformational inhomogeneity and increase the ESPT propensity in the Ca^{2+}-bound state. Since conserved arginine residues (e.g., Arg96 in wtGFP)[3,8] with a positively charged side chain are considered important in stabilizing the charge-transfer excited state of a protein chromophore, we envision that modification of a key residue in the vicinity of the chromophore may provide a directional force to interact with R377 via water bridges and/or electrostatic interactions,[14,49] thus limiting the orientations of the R377 side chain relative

to the chromophore phenolate oxygen in the Ca^{2+}-bound state. The replacement of R377 with a negatively charged residue such as Glu or Asp represents an alternative strategy by maintaining the hydrophilic environment while providing directional H-bonding and proton acceptors to potentially "reroute" the ESPT chain in the Ca^{2+}-bound state, hence making an ratiometric or intensiometric biosensor with improved sensing capabilities.[50,51]

On the other hand, a thiol bridge or some H-bonding partners could be incorporated to restrict the chromophore phase space[52] around the ESPT-prone region so a more homogeneous A* population can effectively proceed to I*. Previous work on the GFP model chromophore such as the widely studied *p*-hydroxybenzylideneimidazolidinone (HBDI) in solution has shown that chromophore twisting around the ethylenic bridge region leads to the dominant energy relaxation pathway (i.e., nonradiative internal conversion from S_1 to S_0),[14,53,54] which is greatly suppressed for the locked chromophores or inside a protein pocket.[10,39,55] The chromophore surroundings can thus be carefully tuned to provide sufficient structural constraints to increase the nonradiative isomerization energy barrier[56,57] so the fluorescence pathway becomes more favored.

In addition, implementing a hydrophilic canonical (e.g., Lys, His) or noncanonical amino acid (NCAA)[58] that interacts with the chromophore from a slightly larger distance could help promote ESPT in a less crowded environment with a higher fluorescence quantum yield, which also reduces the trapped A* population by allowing more efficient relaxation pathways of A*, thereby leading to improved photostability of the overall biosensor. Since the P377R biosensor acts in an excitation ratiometric manner, increasing the B population in the Ca^{2+}-bound state is also beneficial, and the aforementioned strategies are expected to shift the ground state equilibrium from A to B due to a more favorable H-bonding environment with a better positioned and more homogeneous R377 (or another hydrophilic residue after the bioengineering step as stated above) interacting with the

phenolic end of the chromophore. It is interesting to note that a previous two-photon absorption spectroscopic study showed a blue-shifted absorption peak for the lowest-energy band in the one-photon absorption spectrum (see Figure 2a for example) of the anionic form of an enhanced GFP chromophore, which led to a proposed hidden electronic excited state (e.g., S_2) with a large two-photon absorptivity.[59] Though this result was specifically tied to a deprotonated TYG chromophore either in solution or inside enhanced GFP, not the protonated SYG chromophore in a GFP-based calcium biosensor mutant as reported herein, we consider it as further evidence that the elucidation of multidimensional electronic PES of the protein chromophore is non-trivial and requires a careful assessment of the observed spectral data on various time scales and under specific experimental conditions. This exertion is especially pertinent when two-photon absorption is desired for greater penetration depth and/or higher resolutions in advanced bioimaging applications.[51,60]

IV. CONCLUSIONS

Understanding how fluorescent protein based Ca^{2+} biosensors work is of fundamental interest and use for applications in bioimaging and life sciences. In this contribution, we have implemented the tunable FSRS technique, aided by fs-TA and computations, to elucidate how a single-site P377R mutation affects the main function (i.e., fluorescence) of a GFP-based calcium ion biosensor. The Ca^{2+}-free state has a largely homogeneous chromophore environment due to the unrestricted β-barrel opening with labile water molecules and a distant R377 residue. Direct tracking of deprotonated I* species reveals a ~14 ps ESPT reaction and ~4 ps vibrational cooling time constant in the I* state, while the protonated A* species shows biexponential decay time constants of 500 fs and 30 ps. Upon Ca^{2+} binding, R377 impedes the β-barrel opening and yields a more compact biosensor interior with restricted water molecules as the bridge for ESPT and subsequent relaxation. The resultant chromophore population becomes more inhomogeneous: one

subpopulation undergoes faster ESPT to I* than its Ca^{2+}-free counterpart with an 8 ps time constant for green emission, while another subpopulation favors a trapped A* species that yields more emission in the blue. Moreover, the nascent I* population adopts a more twisted conformation as it vibrationally cools and stabilizes within a dynamic H-bonding network before fluorescence, reflected by the correlated Raman marker band frequency dynamics including the ~8 (1) ps red shift of the 1563 cm^{-1} A* (1593 cm^{-1} I*) mode.

The altered reaction pathways underlie the overall decreased green emission with more photodegradation after 400 nm excitation of the Ca^{2+}-bound biosensor, which substantiates the spectroscopy-aided rational design strategies to reduce conformational inhomogeneity by modifying the chromophore-R377 interaction to be more directional, less compact, and with improved plasticity. The incorporation of specific functional groups to the protein chromophore via NCAA methodology and characterization by tunable FSRS technique to dissect fluorescence properties is currently underway in our lab.

Supporting Information. This material is available free of charge on the ACS Publications website at http://pubs.acs.org.

Additional discussion on the significance of this work, Figures S1-S4 on fs-TA dynamics of main SE band and shoulder, target analysis, FSRS baselines and peak line shapes, depiction of the DFT-calculated Raman modes, Table S1 on key Raman mode assignments, additional references, and the full authorship of Gaussian 09 software (PDF)

AUTHOR INFORMATION

Corresponding Author

* E-mail: Chong.Fang@oregonstate.edu. Phone: 541-737-6704.

Present Address

§ W.L.: School of Physical Science and Technology, ShanghaiTech University, Pudong, Shanghai 201210, P. R. China.

Notes

The authors declare no competing financial interest.

ACKNOWLEDGMENTS

This work is supported in part by the NSF CAREER grant (CHE-1455353), NSF grant (MCB-1817949), Oregon Medical Research Foundation New Investigator Grant (2016–2017), and OSU Research Equipment Reserve Fund (Spring 2014) to C.F. The OSU Chemistry Dorothy and Ramon Barnes Graduate Fellowship to S.R.T. is acknowledged (Summer 2018). We thank Dr. Yongxin Zhao and Prof. Robert Campbell (University of Alberta, Canada) for providing the GEM-GECO1-P377R protein biosensor samples, and Dr. Fangyuan Han for LabVIEW and Igor programming.

REFERENCES

(1) Shimomura, O.; Johnson, F. H.; Saiga, Y. Extraction, Purification and Properties of Aequorin, a Bioluminescent Protein from the Luminous Hydromedusan, Aequorea. *J. Cell. Comp. Physiol.* **1962**, *59*, 223-239.

(2) Miyawaki, A.; Llopis, J.; Heim, R.; McCaffery, J. M.; Adams, J. A.; Ikura, M.; Tsien, R. Y. Fluorescent Indicators for Ca^{2+} Based on Green Fluorescent Proteins and Calmodulin. *Nature* **1997**, *388*, 882-887.

(3) Tsien, R. Y. The Green Fluorescent Protein. *Annu. Rev. Biochem.* **1998**, *67*, 509-544.

(4) Prevarskaya, N.; Skryma, R.; Shuba, Y. Calcium in Tumour Metastasis: New Roles for Known Actors. *Nat. Rev. Cancer* **2011**, *11*, 609-618.

(5) Grienberger, C.; Konnerth, A. Imaging Calcium in Neurons. *Neuron* **2012**, *73*, 862-885.

(6) Akerboom, J.; Carreras Calderon, N.; Tian, L.; Wabnig, S.; Prigge, M.; Tolo, J.; Gordus, A.; Orger, M. B.; Severi, K. E.; Macklin, J. J.; et al. Genetically Encoded Calcium Indicators for Multi-Color Neural Activity Imaging and Combination with Optogenetics. *Front. Mol. Neurosci.* **2013**, *6*, 2.

(7) Chattoraj, M.; King, B. A.; Bublitz, G. U.; Boxer, S. G. Ultra-fast Excited State Dynamics in Green Fluorescent Protein: Multiple States and Proton Transfer. *Proc. Natl. Acad. Sci. U. S. A.* **1996**, *93*, 8362-8367.

(8) Brejc, K.; Sixma, T. K.; Kitts, P. A.; Kain, S. R.; Tsien, R. Y.; Ormö, M.; Remington, S. J. Structural Basis for Dual Excitation and Photoisomerization of the *Aequorea victoria* Green Fluorescent Protein. *Proc. Natl. Acad. Sci. U. S. A.* **1997**, *94*, 2306-2311.

(9) Zimmer, M. Green Fluorescent Protein (GFP): Applications, Structure, and Related Photophysical Behavior. *Chem. Rev.* **2002**, *102*, 759-781.

(10) Fang, C.; Frontiera, R. R.; Tran, R.; Mathies, R. A. Mapping GFP Structure Evolution During Proton Transfer with Femtosecond Raman Spectroscopy. *Nature* **2009**, *462*, 200-204.

(11) Meech, S. R. Excited State Reactions in Fluorescent Proteins. *Chem. Soc. Rev.* **2009**, *38*, 2922-2934.

(12) Zhu, L.; Liu, W.; Fang, C. A Versatile Femtosecond Stimulated Raman Spectroscopy Setup with Tunable Pulses in the Visible to Near Infrared. *Appl. Phys. Lett.* **2014**, *105*, 041106.

(13) Dietze, D. R.; Mathies, R. A. Femtosecond Stimulated Raman Spectroscopy. *ChemPhysChem* **2016**, *17*, 1224-1251.

(14) Fang, C.; Tang, L.; Oscar, B. G.; Chen, C. Capturing Structural Snapshots During Photochemical Reactions with Ultrafast Raman Spectroscopy: From Materials Transformation to Biosensor Responses. *J. Phys. Chem. Lett.* **2018**, *9*, 3253–3263.

(15) Frisch, M. J.; Trucks, G. W.; Schlegel, H. B.; Scuseria, G. E.; Robb, M. A.; Cheeseman, J. R.; Scalmani, G.; Barone, V.; Mennucci, B.; Petersson, G. A.; et al. *Gaussian 09,* Revision B.1; Gaussian, Inc.: Wallingford, CT, 2009.

(16) Zhao, Y.; Araki, S.; Wu, J.; Teramoto, T.; Chang, Y.-F.; Nakano, M.; Abdelfattah, A. S.; Fujiwara, M.; Ishihara, T.; Nagai, T.; Campbell, R. E. An Expanded Palette of Genetically Encoded Ca^{2+} Indicators. *Science* **2011**, *333*, 1888-1891.

(17) Oscar, B. G.; Liu, W.; Zhao, Y.; Tang, L.; Wang, Y.; Campbell, R. E.; Fang, C. Excited-State Structural Dynamics of a Dual-Emission Calmodulin-Green Fluorescent Protein Sensor for Calcium Ion Imaging. *Proc. Natl. Acad. Sci. U. S. A.* **2014**, *111*, 10191-10196.

(18) Tang, L.; Liu, W.; Wang, Y.; Zhao, Y.; Oscar, B. G.; Campbell, R. E.; Fang, C. Unraveling Ultrafast Photoinduced Proton Transfer Dynamics in a Fluorescent Protein Biosensor for Ca^{2+} Imaging. *Chem. Eur. J.* **2015**, *21*, 6481-6490.

(19) Tachibana, S. R.; Tang, L.; Wang, Y.; Zhu, L.; Liu, W.; Fang, C. Tuning Calcium Biosensors with a Single-Site Mutation: Structural Dynamics Insights from Femtosecond Raman Spectroscopy. *Phys. Chem. Chem. Phys.* **2017**, *19*, 7138-7146.

(20) Tang, L.; Wang, Y.; Liu, W.; Zhao, Y.; Campbell, R. E.; Fang, C. Illuminating Photochemistry of an Excitation Ratiometric Fluorescent Protein Calcium Biosensor. *J. Phys. Chem. B* **2017**, *121*, 3016-3023.

(21) Berera, R.; van Grondelle, R.; Kennis, J. T. M. Ultrafast Transient Absorption Spectroscopy: Principles and Application to Photosynthetic Systems. *Photosynth. Res.* **2009**, *101*, 105-118.

(22) McCamant, D. W.; Kukura, P.; Yoon, S.; Mathies, R. A. Femtosecond Broadband Stimulated Raman Spectroscopy: Apparatus and Methods. *Rev. Sci. Instrum.* **2004**, *75*, 4971-4980.

(23) Liu, W.; Wang, Y.; Tang, L.; Oscar, B. G.; Zhu, L.; Fang, C. Panoramic Portrait of Primary Molecular Events Preceding Excited State Proton Transfer in Water. *Chem. Sci.* **2016**, *7*, 5484-5494.

(24) Tang, L.; Liu, W.; Wang, Y.; Zhu, L.; Han, F.; Fang, C. Ultrafast Structural Evolution and Chromophore Inhomogeneity inside a Green-Fluorescent-Protein-Based Ca^{2+} Biosensor. *J. Phys. Chem. Lett.* **2016**, *7*, 1225-1230.

(25) Tang, L.; Wang, Y.; Zhu, L.; Kallio, K.; Remington, S. J.; Fang, C. Photoinduced Proton Transfer Inside an Engineered Green Fluorescent Protein: A Stepwise-Concerted-Hybrid Reaction. *Phys. Chem. Chem. Phys.* **2018**, *20*, 12517–12526.

(26) Fang, C.; Senes, A.; Cristian, L.; DeGrado, W. F.; Hochstrasser, R. M. Amide Vibrations Are Delocalized Across the Hydrophobic Interface of a Transmembrane Helix Dimer. *Proc. Natl. Acad. Sci. U. S. A.* **2006**, *103*, 16740-16745.

(27) Laptenok, S. P.; Lukacs, A.; Gil, A.; Brust, R.; Sazanovich, I. V.; Greetham, G. M.; Tonge, P. J.; Meech, S. R. Complete Proton Transfer Cycle in GFP and Its T203V and S205V Mutants. *Angew. Chem. Int. Ed.* **2015**, *54*, 9303-9307.

(28) Laptenok, S. P.; Gil, A. A.; Hall, C. R.; Lukacs, A.; Iuliano, J. N.; Jones, G. A.; Greetham, G. M.; Donaldson, P.; Miyawaki, A.; Tonge, P. J.; Meech, S. R. Infrared Spectroscopy Reveals

Multi-Step Multi-Timescale Photoactivation in the Photoconvertible Protein Archetype Dronpa. *Nat. Chem.* **2018**, *10*, 845-852.

(29) Nibbering, E. T. J.; Fidder, H.; Pines, E. Ultrafast Chemistry: Using Time-Resolved Vibrational Spectroscopy for Interrogation of Structural Dynamics. *Annu. Rev. Phys. Chem.* **2005**, *56*, 337-367.

(30) McAnaney, T. B.; Park, E. S.; Hanson, G. T.; Remington, S. J.; Boxer, S. G. Green Fluorescent Protein Variants as Ratiometric Dual Emission pH Sensors. 2. Excited-State Dynamics. *Biochemistry* **2002**, *41*, 15489-15494.

(31) Henderson, J. N.; Remington, S. J. Crystal Structures and Mutational Analysis of amFP486, A Cyan Fluorescent Protein from Anemonia majano. *Proc. Natl. Acad. Sci. U. S. A.* **2005**, *102*, 12712-12717.

(32) Spry, D. B.; Fayer, M. D. Charge Redistribution and Photoacidity: Neutral versus Cationic Photoacids. *J. Chem. Phys.* **2008**, *128*, 084508.

(33) Olsen, S. Locally-Excited (LE) versus Charge-Transfer (CT) Excited State Competition in a Series of Para-Substituted Neutral Green Fluorescent Protein (GFP) Chromophore Models. *J. Phys. Chem. B* **2015**, *119*, 2566-2575.

(34) Chen, C.; Liu, W.; Baranov, M. S.; Baleeva, N. S.; Yampolsky, I. V.; Zhu, L.; Wang, Y.; Shamir, A.; Solntsev, K. M.; Fang, C. Unveiling Structural Motions of a Highly Fluorescent Superphotoacid by Locking and Fluorinating the GFP Chromophore in Solution. *J. Phys. Chem. Lett.* **2017**, *8*, 5921–5928.

(35) Lochbrunner, S.; Wurzer, A. J.; Riedle, E. Ultrafast Excited-State Proton Transfer and Subsequent Coherent Skeletal Motion of 2-(2'-hydroxyphenyl)benzothiazole. *J. Chem. Phys.* **2000**, *112*, 10699-10702.

(36) Spillane, K. M.; Dasgupta, J.; Lagarias, J. C.; Mathies, R. A. Homogeneity of Phytochrome Cph1 Vibronic Absorption Revealed by Resonance Raman Intensity Analysis. *J. Am. Chem. Soc.* **2009**, *131*, 13946-13948.

(37) Snellenburg, J. J.; Laptenok, S.; Seger, R.; Mullen, K. M.; van Stokkum, I. H. M. Glotaran: A Java-Based Graphical User Interface for the R Package TIMP. *J. Stat. Softw.* **2012**, *49*, 1-22.

(38) Tang, L.; Zhu, L.; Wang, Y.; Fang, C. Uncovering the Hidden Excited State toward Fluorescence of an Intracellular pH Indicator. *J. Phys. Chem. Lett.* **2018**, *9*, 4969-4975.

(39) Tang, L.; Zhu, L.; Taylor, M. A.; Wang, Y.; Remington, S. J.; Fang, C. Excited State Structural Evolution of a GFP Single-Site Mutant Tracked by Tunable Femtosecond-Stimulated Raman Spectroscopy. *Molecules* **2018**, *23*, 2226.

(40) Mizutani, Y.; Kitagawa, T. Direct Observation of Cooling of Heme Upon Photodissociation of Carbonmonoxy Myoglobin. *Science* **1997**, *278*, 443-446.

(41) Liu, W.; Tang, L.; Oscar, B. G.; Wang, Y.; Chen, C.; Fang, C. Tracking Ultrafast Vibrational Cooling During Excited State Proton Transfer Reaction with Anti-Stokes and Stokes Femtosecond Stimulated Raman Spectroscopy. *J. Phys. Chem. Lett.* **2017**, *8*, 997–1003.

(42) Tang, L.; Wang, Y.; Zhu, L.; Lee, C.; Fang, C. Correlated Molecular Structural Motions for Photoprotection After Deep-UV Irradiation. *J. Phys. Chem. Lett.* **2018**, *9*, 2311-2319.

(43) Wang, Y.; Tang, L.; Liu, W.; Zhao, Y.; Oscar, B. G.; Campbell, R. E.; Fang, C. Excited State Structural Events of a Dual-Emission Fluorescent Protein Biosensor for Ca^{2+} Imaging Studied by Femtosecond Stimulated Raman Spectroscopy. *J. Phys. Chem. B* **2015**, *119*, 2204-2218.

(44) Lee, S.-Y.; Zhang, D.; McCamant, D. W.; Kukura, P.; Mathies, R. A. Theory of Femtosecond Stimulated Raman Spectroscopy. *J. Chem. Phys.* **2004**, *121*, 3632-3642.

(45) Oscar, B. G.; Chen, C.; Liu, W.; Zhu, L.; Fang, C. Dynamic Raman Line Shapes on an Evolving Excited-State Landscape: Insights from Tunable Femtosecond Stimulated Raman Spectroscopy. *J. Phys. Chem. A* **2017**, *121*, 5428-5441.

(46) Ellis, S. R.; Hoffman, D. P.; Park, M.; Mathies, R. A. Difference Bands in Time-Resolved Femtosecond Stimulated Raman Spectra of Photoexcited Intermolecular Electron Transfer from Chloronaphthalene to Tetracyanoethylene. *J. Phys. Chem. A* **2018**, *122*, 3594-3605.

(47) Agmon, N. Elementary Steps in Excited-State Proton Transfer. *J. Phys. Chem. A* **2005**, *109*, 13-35.

(48) Pecourt, J.-M. L.; Peon, J.; Kohler, B. DNA Excited-State Dynamics: Ultrafast Internal Conversion and Vibrational Cooling in a Series of Nucleosides. *J. Am. Chem. Soc.* **2001**, *123*, 10370-10378.

(49) Park, J. W.; Rhee, Y. M. Electric Field Keeps Chromophore Planar and Produces High Yield Fluorescence in Green Fluorescent Protein. *J. Am. Chem. Soc.* **2016**, *138*, 13619-13629.

(50) Shu, X.; Kallio, K.; Shi, X.; Abbyad, P.; Kanchanawong, P.; Childs, W.; Boxer, S. G.; Remington, S. J. Ultrafast Excited-State Dynamics in the Green Fluorescent Protein Variant S65T/H148D. 1. Mutagenesis and Structural Studies. *Biochemistry* **2007**, *46*, 12005-12013.

(51) Wu, J.; Abdelfattah, A. S.; Miraucourt, L. S.; Kutsarova, E.; Ruangkittisakul, A.; Zhou, H.; Ballanyi, K.; Wicks, G.; Drobizhev, M.; Rebane, A.; Ruthazer, E. S.; Campbell, R. E. A Long Stokes Shift Red Fluorescent Ca^{2+} Indicator Protein for Two-Photon and Ratiometric Imaging. *Nat. Commun.* **2014**, *5*, 5262.

(52) Burgie, E. S.; Vierstra, R. D. Phytochromes: An Atomic Perspective on Photoactivation and Signaling. *Plant Cell* **2014**, *26*, 4568-4583.

(53) Mandal, D.; Tahara, T.; Meech, S. R. Excited-State Dynamics in the Green Fluorescent Protein Chromophore. *J. Phys. Chem. B* **2004**, *108*, 1102-1108.

(54) Usman, A.; Mohammed, O. F.; Nibbering, E. T. J.; Dong, J.; Solntsev, K. M.; Tolbert, L. M. Excited-State Structure Determination of the Green Fluorescent Protein Chromophore. *J. Am. Chem. Soc.* **2005**, *127*, 11214-11215.

(55) Baranov, M. S.; Lukyanov, K. A.; Borissova, A. O.; Shamir, J.; Kosenkov, D.; Slipchenko, L. V.; Tolbert, L. M.; Yampolsky, I. V.; Solntsev, K. M. Conformationally Locked Chromophores as Models of Excited-State Proton Transfer in Fluorescent Proteins. *J. Am. Chem. Soc.* **2012**, *134*, 6025-6032.

(56) Polyakov, I. V.; Grigorenko, B. L.; Epifanovsky, E. M.; Krylov, A. I.; Nemukhin, A. V. Potential Energy Landscape of the Electronic States of the GFP Chromophore in Different Protonation Forms: Electronic Transition Energies and Conical Intersections. *J. Chem. Theory Comput.* **2010**, *6*, 2377-2387.

(57) Kumpulainen, T.; Lang, B.; Rosspeintner, A.; Vauthey, E. Ultrafast Elementary Photochemical Processes of Organic Molecules in Liquid Solution. *Chem. Rev.* **2017**, *117*, 10826-10939.

(58) Peeler, J. C.; Mehl, R. A. Site-Specific Incorporation of Unnatural Amino Acids as Probes for Protein Conformational Changes. In *Unnatural Amino Acids: Methods and Protocols*; Pollegioni, L., Servi, S., Eds.; Humana Press: New York, NY, 2012; pp 125-134.

(59) Hosoi, H.; Yamaguchi, S.; Mizuno, H.; Miyawaki, A.; Tahara, T. Hidden Electronic Excited State of Enhanced Green Fluorescent Protein. *J. Phys. Chem. B* **2008**, *112*, 2761-2763.

(60) Drobizhev, M.; Makarov, N. S.; Tillo, S. E.; Hughes, T. E.; Rebane, A. Two-Photon Absorption Properties of Fluorescent Proteins. *Nat. Meth.* **2011**, *8*, 393-399.

TOC GRAPHIC

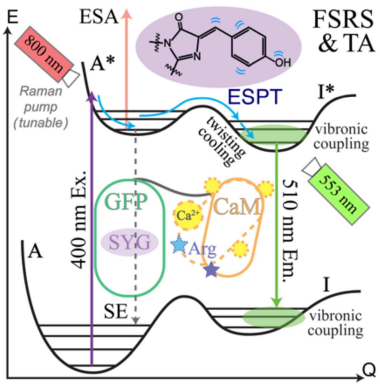
E
ESA
FSRS
& TA
800 nm
Raman
pump
(tunable)
A*
ESPT
I*
twisting
cooling
vibronic
coupling
553 nm
400 nm Ex.
GFP
SYG
Ca2+
CaM
Arg
510 nm Em.
A
SE
I
vibronic
coupling
Q